Journal Name RSCPublishing

ARTICLE

Hierarchically porous N-F codoped TiO_2 hollow spheres prepared via an in situ bubbling method for dye-sensitized solar cells

Cite this: DOI: 10.1039/x0xx00000x

Received 00th January 2012,
Accepted 00th January 2012

DOI: 10.1039/x0xx00000x

www.rsc.org/

Bing-Xin Lei, Li-Li Zeng, Ping Zhang, Xiao-Feng Zheng, Yan-Shan Wu, Jun Fu and Zhen-Fan Sun*

Hierarchically porous N-F codoped TiO_2 hollow spheres with diameter of 0.8-1.8 μm and shell thickness of 250 nm are synthesized via an in situ bubbling method. Although the photoelectrode film constructed with the hierarchically porous N-F codoped TiO_2 hollow spheres possesses a lower specific surface area than that of P25 nanocrystallites and thus achieves less dye adsorption, it may generate effective light scattering and therefore enhance the light harvesting efficiency, leading to higher power conversion efficiency (6.59%). The double layered DSSC with the hierarchically porous N-F codoped TiO_2 hollow spheres as the top layer and P25 as the bottom layer is constructed and a 7.36% solar energy conversion efficiency is demonstrated, indicating a 10% improvement compared with the P25 cell of 6.65%. The improved photovoltaic performance of the double layered DSSC is primarily due to the effective suppression of the back reaction of the injected electron with the I_3^- in the electrolyte by decreasing the surface charge trap-site density of the photoanode and excellent light scatter ability.

1. Introduction

Since the breakthrough work by Grätzel in 1991, dye-sensitized solar cells (DSSCs) have been attracting ever-increasing attention from researchers in both academia and industry and have been considered a promising renewable photovoltaic technology because of their low cost and facile fabrication procedure.[1] Although the record-setting efficiency of 13% achieved to date has been attributed to mesoporous TiO_2 nanocrystalline based DSSCs,[2] researchers made lots of efforts on all relevant aspects of DSSCs to further enhance the performance, such as optimizing sensitizers, redox electrolytes, counter electrodes and photoanode materials.[2-6] At the heart of the DSSC is a nanocrystalline semiconductor oxide (typically TiO_2, ZnO, etc.) film, whose structure and morphology play a critical role in determining the performance of DSSCs. Since the nanosized particles (~10-30 nm) are too weak to scatter the visible light, while large particles with flat surfaces usually decrease the dye loading due to their much lower surface area, the hierarchically structured materials consisting of smaller building blocks, have been widely investigated recently as photoanode materials for DSSCs to provide both high dye adsorption and good light scattering abilities. Thus, a further improvement of DSSCs performance could be achieved by introducing some hierarchically hollow TiO_2 nanostructures (TiO_2 hollow spheres[5] and TiO_2 hollow nanoplates[6]) as scattering centers, with even stronger light scattering effect and efficient electrolyte diffusion ability. Moreover, the multiple-reflection effect occurring inside the interior cavities could trap the incident light in the photoanode for a longer duration, which brought forth more opportunities for light absorption.[7, 8]

TiO_2 hollow spheres have attracted extensive attention due to their well-defined interior voids, higher specific surface area, lower density, greater delivering ability, better permeation and stronger multiple-reflection effect compared to solid ones. TiO_2 hollow structured microspheres have been widely investigated as the photoanode materials in DSSC since they can effectively scatter the visible light, facilitate the infiltration of electrolyte solution and reduce the interface recombination by decreasing the surface charge trap-site density.[9] Koo et al. obtained over 10% efficiency for a DSSC with a nano-embossed hollow spherical TiO_2 particulate film as an overlayer on a nanocrystalline TiO_2 film.[9] Recently, much attention has been paid to the utilization of TiO_2 hollow spheres as photoanodes in DSSCs.[5, 10-15]

A general approach to fabricate TiO_2 hollow spheres accompanies the use of removable or sacrificial templates, such as polystyrene beads,[16, 17] carbonaceous polysaccharide microspheres,[18] silica colloid spheres,[19] surfactants,[20] emulsions[21] and so on. They suffer from many disadvantages such as high cost, tedious procedure and collapse of the hollow structure when removing the templates, which can hinder the large-scale industrial applications. Therefore, it is highly desirable to develop a novel approach for the fabrication of hierarchical TiO_2 hollow spheres with template-free, surfactant-free, simple manipulation, low cost and large scale production.

Herein, we developed a facile strategy for the preparation of hierarchical N-F codoped TiO_2 hollow spheres using CO_2 bubble method, which was produced by the decomposition of urea under mild hydrothermal conditions. This unique structure with diameter ranged from 0.8 to 1.8 μm was assembled from well-crystallized nanoparticles. Moreover, nitrogen adsorption isotherms analysis demonstrated that the obtained hierarchical N-F codoped TiO_2 hollow spheres had a specific surface area of 29.845 m^2 g^{-1}. Furthermore, we used these hierarchical N-F codoped TiO_2 hollow microspheres as the scattering layer to balance the dye adsorption and scattering effect in DSSCs and a 7.30% solar energy conversion efficiency was demonstrated.

2. Experimental section

2.1 Materials

Ammonium hexafluorotitanate ($(NH_4)_2TiF_6$, AR) and polyethylene glycol 600 (PEG-600) were purchased from Aladdin Chemical Reagent Co., Ltd. (Shanghai, China). Urea (AR) was obtained from Sinopharm Chemical Reagent Co., Ltd. (Shanghai, China). All of the chemicals were used without further purification. The substrates were commercial FTO (glass/SnO_2:F, 14 Ω/□) from Nippon Sheet Glass Co., Ltd.

2.2 Preparation of hierarchically porous N-F codoped TiO_2 hollow spheres

In a typical synthesis, 0.1979 g of $(NH_4)_2TiF_6$ and 2.7027 g of urea were dissolved into 40.0 mL of H_2O, adding 1.0 mL of PEG-600 drop by drop. After being stirred for 30 min, the clear solution was then transferred into a Teflon-lined stainless-steel autoclave with 50 mL capacity. Then, the autoclave was kept at 180 ^oC for 12 h in an electric oven. After the reaction, the resultant products were collected by centrifugation, rinsed thoroughly with deionized water and ethanol several times to remove impurities, and dried in air at 70 °C for 6 h.

2.3 Characterizations of hierarchically porous N-F codoped TiO_2 hollow spheres

The phase purity of the products was characterized by X-ray diffraction (XRD) on a Bruker D8 Advance X-ray diffractometer using Cu Kα radiation (λ=1.5418 Å). The field emission scanning electron microscopy (FE-SEM, JSM-7100F) was performed to characterize the morphology and size. The transmission electron microscopy (TEM) and high-resolution transmission electron microscopy (HRTEM) were performed on a JEOL-2010 HR transmission electron microscope. To determine the Brunauer-Emmett-Teller (BET) specific surface area and pore size distribution of the samples, the N_2 sorption measurements were performed by using an Autosorb-iQ surface area analyzer (Quantachrome Instruments US). X-ray photoelectron spectroscopy (XPS) measurements were taken by using a spectrometer (Thermo Fisher Scientific, ESCALAB 250) with a monochromic Al Ka source at 1486.7 eV, at a voltage of 15 kV and an emission current of 10 mA.

2.4 Preparation of TiO_2 working electrode

The paste of hierarchically porous N-F codoped TiO_2 hollow spheres was prepared according to the reference.[22] Briefly, the TiO_2 powder (1.0 g) was dispersed in the mixture of ethanol (1.00 mL) and acetic acid (0.20 mL) and ground for 5 min. Then, 5.00 mL of ethanol and 3.00 g of terpineol were introduced into the above mixture and ground for 5 min. Subsequently, 3.00 mL of ethanol and 0.40 g of ethyl cellulose were added and the mixture was ground for another 30 min was sonicated for 5 min in an ultrasonic bath. The paste of P25 nanoparticles (Degussa) was prepared by the same method. Finally, the resulting colloidal suspension was deposited on FTO glass with an active area of 0.16 cm^2, by using the screen-printing technique. The film thickness was controlled by repeating the printing process. Prior to the screen-printing, FTO glass substrates were ultrasonically cleaned by deionized water, acetone and ethanol, successively. TiO_2 films were annealed by a calcination process in the furnace through a programmed temperature process at 325 °C for 5 min, at 375 °C for 5 min, at 450 °C for 15 min, and then at 500 °C for 15 min.

2.5 Fabrication and photovoltaic measurements of DSSCs

The as-prepared TiO_2 films were treated with 40 mM $TiCl_4$ aqueous solution at 70 °C for 30 min, followed by sintering at 520 °C for 30 min. After cooling down to ~80 °C, the TiO_2 films were immediately immersed into 0.5 mM N719 dye ($[(C_4H_9)_4N]_2[Ru(II)L_2(NCS)_2]$, where L = 2,2'-bipyridyl-4, 4'-dicarboxylic acid, Solaronix SA, Switzerland) in acetonitrile/tert-butanol (v/v, 1:1) for 16 h at room temperature. Afterwards, these films were rinsed with acetonitrile in order to remove physically adsorbed N719 dye molecules. The Pt counter electrodes were fabricated by thermal-deposition of H_2PtCl_6 solution (5 mM in isopropanol) onto FTO glass. Finally, the dye adsorbed TiO_2 photoanode and Pt counter electrode were assembled into a sandwich type cell. The electrolyte solution containing 0.03 M I_2, 0.05 M LiI, 0.6 M 1-methyl-3-propylimidazolium iodide (PMII), 0.10 M guanidinium thiocyanate, and 0.5 M tert-butylpyridine in acetonitrile and valeronitrile (v/v, 85:15), was introduced into the cell from a drilled hole on the counter electrode.

The photocurrent-voltage characteristics of DSSCs were recorded using a Keithley model 2400 digital source meter under one sun AM 1.5 G (100 mW cm^{-2}) illumination with a solar light simulator (Oriel, Model: 94041A). A 450 W Xenon lamp was served as a light source and its incident light intensity was calibrated with a NREL-calibrated Si solar cell to accurately simulate the full-sun intensity (100 mW cm^{-2}). The thicknesses of TiO_2 films were measured by using a D-100 profilometer of KLA-Tencor. The electrochemical impedance spectroscopy (EIS) measurements were performed with a Zennium electrochemical workstation (ZAHNER) with the frequency range from 10 mHz to 1000 kHz. The magnitude of the alternative signal was 10 mV. The impedance measurements were carried out under forward bias of -0.830 V in the dark. Incident photon to current conversion efficiency (IPCE) was measured on photo current spectra system of CIMPS (CIMPS-PCS) with tunable light source (TLS03). In order to calculate the amount of dye in the TiO_2 electrode, we immersed the dye-adsorbed TiO_2 films into 0.1 M NaOH aqueous solution and measured the concentration of desorbed dye on a UV-Vis-NIR spectrophotometer (UV-1901, Beijing Purkinje General Instrument Co. Ltd., China), and the diffuse-reflectance spectra of the TiO_2 films were recorded on the same UV-Vis spectrophotometer at the same time.

3. Results and discussion

The crystal structure of the obtained TiO_2 products was investigated with XRD method. Fig. 1 shows a typical XRD pattern of the as-prepared hierarchically porous N-F codoped TiO_2 hollow spheres. It can be seen that all diffraction peaks of the as-prepared hierarchically porous N-F codoped TiO_2 hollow spheres can coincidently be indexed to the pure anatase phase TiO_2 (JCPDS card No. 21-1272, a=3.79 Å and c=9.51 Å) and no other phases or impurities are observed. For instance, four peaks located at 2θ= 25.3°, 37.8°, 48.05°, and 55.06° could be attributed to (101), (004), (200) and (211) crystal planes of anatase TiO_2, respectively. The sharp diffraction peaks and high intensity indicate the good crystallinity of the as-prepared hierarchically porous N-F codoped TiO_2 hollow spheres.

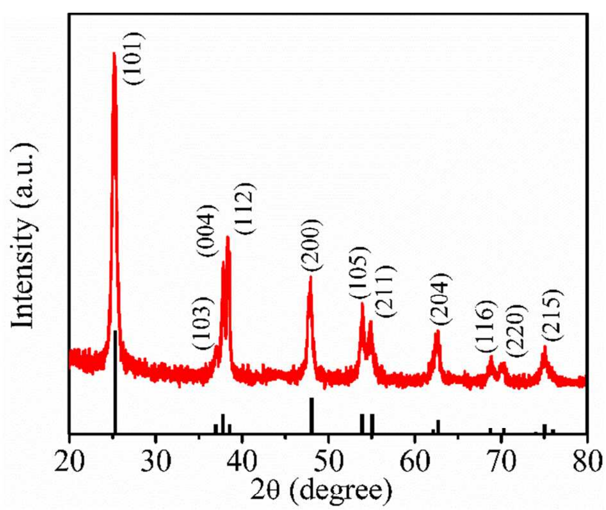

Fig. 1 XRD pattern of the hierarchical porous N-F codoped TiO_2 hollow spheres via a simple hydrothermal method at 180 °C for 12 h.

The crystallite size is estimated using the Scherrer equation:[23]

$$D = 0.9\lambda/\beta\cos\theta \quad (1)$$

where λ, β, and θ represent the wavelength of the X-ray source, the full width at half maximum (FWHM) and the Bragg angle, respectively. The crystallite size estimated from the (101) peak is about 13.8 nm, implying that the as-prepared hierarchically porous N-F codoped TiO_2 hollow spheres are constructed with the nanosized TiO_2 particles.

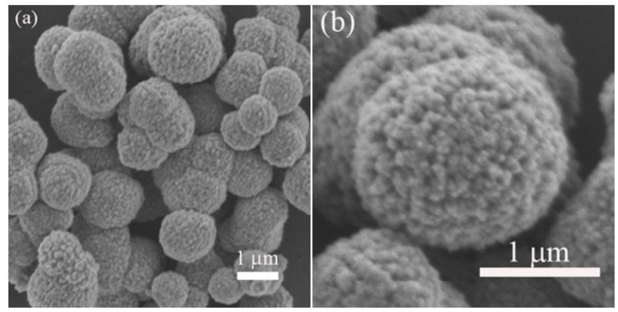

Fig. 2 FE-SEM images of the hierarchically porous N-F codoped TiO_2 hollow spheres prepared via a simple hydrothermal method at 180 °C for 12 h.

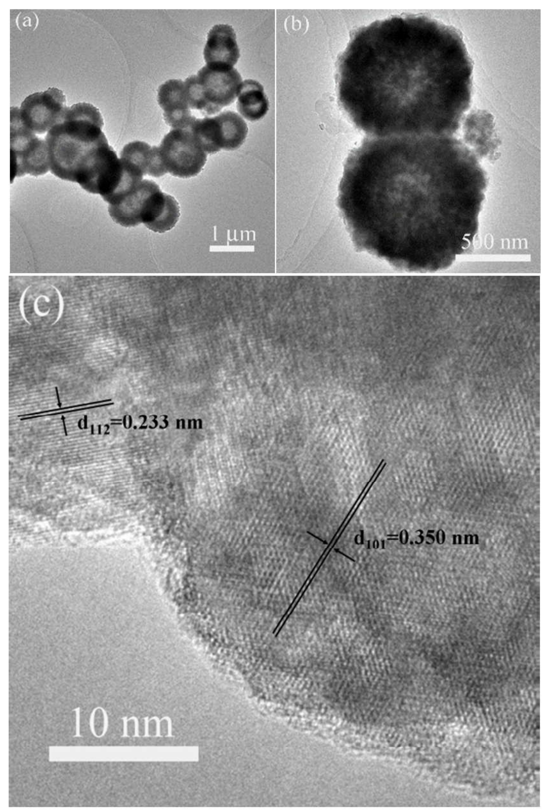

Fig. 3 TEM (a, b) and HRTEM (c) images of the as-prepared hierarchically porous N-F codoped TiO_2 hollow spheres.

The morphology and structure of the as-prepared TiO_2 products were observed by FE-SEM. Fig. 2a is a typically low magnification FE-SEM image of the as-prepared TiO_2 samples, and it is evident from Fig. 2a that the products contain a large quantity of rough spherical particles with diameter ranged from 0.8 to 1.8 μm. In order to observe the surface structure clearly, the higher-magnification FE-SEM image in Fig. 2b shows that the as-prepared TiO_2 samples consist of TiO_2 nanoparticles and we can see the rough surface with lots of holes. These nanoparticles assemble together to form the hierarchical architecture. This architecture is an ideal framework for electrolyte diffusion.

Further the microstructure details of the as-synthesized hierarchically porous N-F codoped TiO_2 hollow spheres can be seen in the TEM and HRTEM images. Fig. 3a shows a typical TEM image of the as-prepared TiO_2 spheres, which reveals the hollow nature of the product. A strong contrast difference between the dark edges and pale centers indicates that each TiO_2 microsphere has a hollow interior in the center. The diameter of hollow interiors is about 250-900 nm, and the thickness of the shell is estimated to be about 250 nm (Fig. 3a). From the enlarged TEM image (Fig. 3b), we can observe that the hollow spheres are surrounded by nanoparticles. Fig. 3c shows a high-resolution TEM (HRTEM) image of a single TiO_2 nanoparticle from the shell of the hollow sphere, confirming that the hierarchically porous N-F codoped TiO_2 hollow spheres are composed of single crystalline anatase TiO_2 nanoparticles. The interplanar spacings of these crystal planes are 0.350 and 0.233 nm, corresponding to the (101) and (112) planes of anatase TiO_2, respectively, which are in good accordance with the results of the XRD pattern (Fig. 1).

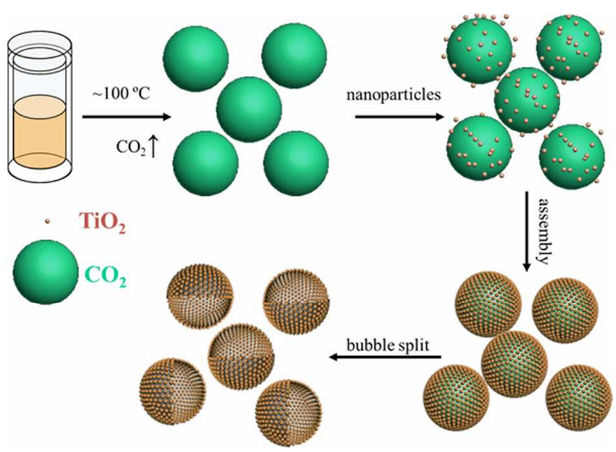

Scheme 1 Illustration of the formation process of hierarchical N-F codoped TiO_2 hollow spheres.

Based on the FE-SEM and TEM observations, the formation of these N-F codoped TiO_2 hollow spheres can be explained the CO_2 bubbling method (Scheme 1). As we know, urea can decompose thermally at a relatively low temperature (below 100 °C) while releasing CO_2 bubbles and increasing the pH of the solution,[24] thereby promoting the precipitation of TiO_2. The in situ generated CO_2 bubbles induce the hollow nanostructure, in which small TiO_2 nanoparticles generated in the reaction could aggregate around the CO_2-liquid interface. As the reaction proceeded, TiO_2 spheres with holes were formed. However, no products were obtained without the addition of urea. A very similar formation mechanism of hollow spheres based on bubble method was also proposed by other research groups.[25-27] During this process, the major chemical reactions in the aqueous solution could be formulated as follows:

$$CO(NH_2)_2 + 3H_2O \rightarrow CO_2 + 2NH_4^+ + 2OH^- \quad (2)$$

$$(NH_4)_2TiF_6 + 6OH^- \rightarrow TiO_2 + 2NH_3 + 4H_2O + 6F^- \quad (3)$$

Furthermore, the microstructural characteristics of the hierarchically porous N-F codoped TiO_2 hollow spheres are further confirmed by the nitrogen adsorption-desorption analysis. Fig. 4 shows the nitrogen adsorption-desorption isotherms and the corresponding pore size distribution for hierarchically porous N-F codoped TiO_2 hollow spheres. Fig. 4 exhibits a type IV isotherm with a clear type H3 hysteresis, typical for mesoporous materials. The hierarchically porous N-F codoped TiO_2 hollow spheres had a BET specific surface area of 29.845 m^2 g^{-1}, which is much lower than that of the commercial P25 (54.214 m^2 g^{-1}). The sample shows bimodal mesopore size distributions (inset in Fig. 4), that is, smaller mesopores with peak pore diameters of ca. 1.91 nm and bigger mesopores with peak pore diameters about 8.47 nm. This bimodal pore-size distribution is ascribed to two different pores: finer intra-aggregated pore within the agglomerated particles and large inter-aggregated pore produced by inter-aggregated secondary particles.[28-30] The hierarchically porous structure of N-F codoped TiO_2 hollow spheres could facilitate electrolyte diffusion and dye loading and enhance light harvesting efficiency, which make potentially useful for application such as DSSCs.

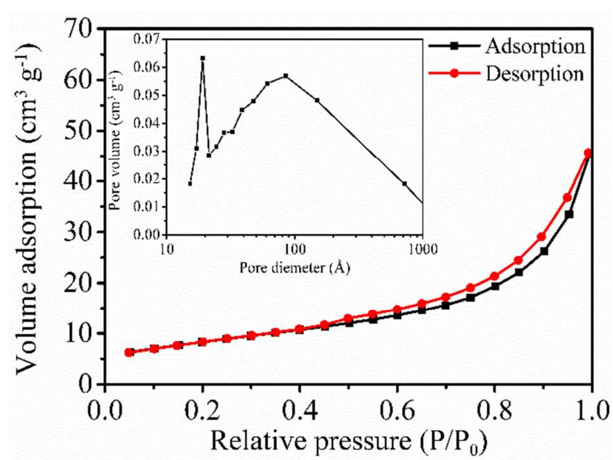

Fig. 4 Nitrogen adsorption-desorption isotherm curves and pore size distribution (inset) of the as-prepared hierarchically porous N-F codoped TiO_2 hollow spheres.

Fig. 5a shows the XPS survey spectrum of the as-prepared hierarchically porous N-F codoped TiO_2 hollow spheres. It is found that the as-prepared hierarchically porous TiO_2 hollow spheres contain only Ti, O, N and F. As shown in Fig. 5b, the peak at 684.4 eV could be assigned to F^- ions physically adsorbed on the surface of TiO_2. Based on XPS results, the content of F atoms are 2.0 at. %. Fig. 5c shows the high-resolution XPS spectra of N 1s region. The nitrogen located at 400 eV is assigned to the nitrogen atoms existing interstitially in the TiO_2 matrices. The N doping level of this sample is about 1 at. %, estimated from the XPS data. The reduction in defect density of the TiO_2 hollow spheres by N and F co-doping will be a benefit for electron transporting in TiO_2 hollow spheres.

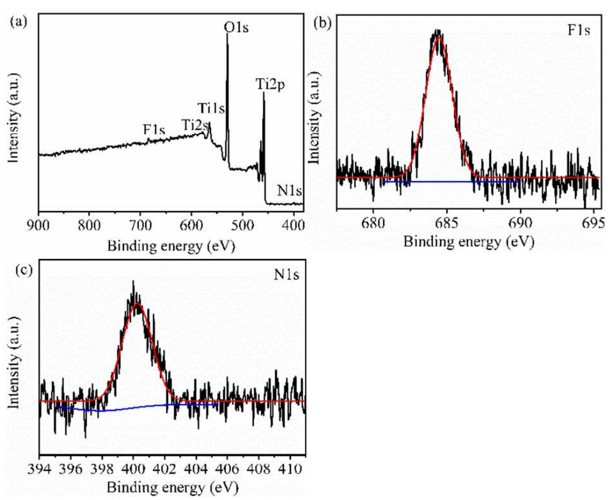

Fig. 5. XPS spectra of (a) survey spectrum, (b) F1s and (c) N1s for the as-prepared hierarchically porous N-F codoped TiO_2 hollow spheres.

In order to investigate the DSSCs performance of the hierarchically porous N-F codoped TiO_2 hollow spheres, we compared three types of cells with different film structures. The bilayer film was constructed by printing a layer (~4.0 μm) of the hierarchically porous N-F codoped TiO_2 hollow spheres which was employed as a scattering layer on the top of a layer (~12.0 μm) of commercial P25 nanocrystals (12.0 μm P25 + 4.0 μm N-F codoped TiO_2 hollow spheres, labeled as Film P25+THS). For comparison, the single layer films consisting of P25 nanoparticles and hierarchically porous N-F codoped TiO_2 hollow spheres with a thickness of~16.0 μm were also fabricated (~16.0 μm P25, labeled as Film P25; ~16.0 μm N-F codoped TiO_2 hollow spheres, labeled as Film THS). Moreover, the corresponding DSSCs assembled from these films were labeled as Cell P25+THS, Cell P25, and Cell-THS, respectively.

The photocurrent density-voltage (*J-V*) curves of DSSCs based on the three types of films (Film P25, Film THS, and Film P25+THS) are shown in Fig. 6. The detailed photovoltaic parameters derived from the *J-V* curves are summarized in Table 1, including open-circuit voltage (V_{oc}), short-circuit current density (J_{sc}), fill factor (*FF*) and power conversion efficiency (η) of these cells. As shown in Fig. 6 and Table 1, the *FF* of the three types of DSSCs based on the different photoanodes doesn't show any obvious changes. It can be seen that the V_{oc} values of Cell THS (V_{oc}=0.865 V) and Cell P25+THS (V_{oc}=0.834 V) are comparatively higher than that of Cell P25 (V_{oc}=0.809 V). The higher V_{oc} values of Cell THS and Cell P25+THS imply that the recombination between the electrons in the hierarchically porous N-F codoped TiO_2 hollow spheres electrode and I_3^- in the electrolyte is suppressed due to the smaller surface area of the hierarchically porous N-F codoped TiO_2 hollow sphere electrode compared with that of the commercial P25 nanocrystalline electrode.[31] In addition, we further investigated the origin and evidence for the increased V_{oc} of Cell THS and Cell P25+THS by performing the dark current potential scans (as shown in Fig. 7). As can be seen from Fig. 7, the dark current onset of Cell THS shifts to a higher potential and produces the smallest dark current at the same potential above 0.6 V, while Cell P25 produces a highest dark current. With the decrease of the dark current, the charge recombination between the electrolyte and transferred electrons could be reduced and the V_{oc} is improved. Compared to Cell P25, the V_{oc} of Cell THS and Cell P25+THS improve by 56 mV and 25 mV. However, Cell THS displays a little lower J_{sc} value of 10.51 mA cm^{-2} than the J_{sc} value of 11.34 mA cm^{-2} for Cell P25. These results lead to a η value of 6.59% for Cell THS, which is all quite close to the η value of 6.65% for Cell P25. The hierarchically porous N-F codoped TiO_2 hollow structure electrode exhibits a performance comparable with that of conventional P25 electrode. When the as-prepared hierarchically porous N-F codoped TiO_2 hollow spheres are deposited to form a scattering layer, the J_{sc} value of the Cell P25+THS is increased to 12.35 mA cm^{-2} and the η value of the Cell P25+THS was improved to 7.36%. Considering the small change in the dye loading amount of Film P25+THS (13.3×10^{-8} mol cm^{-2}), the main function of hierarchically porous N-F codoped TiO_2 hollow spheres is not to produce photocurrent itself but to scatter the incident light backwards.

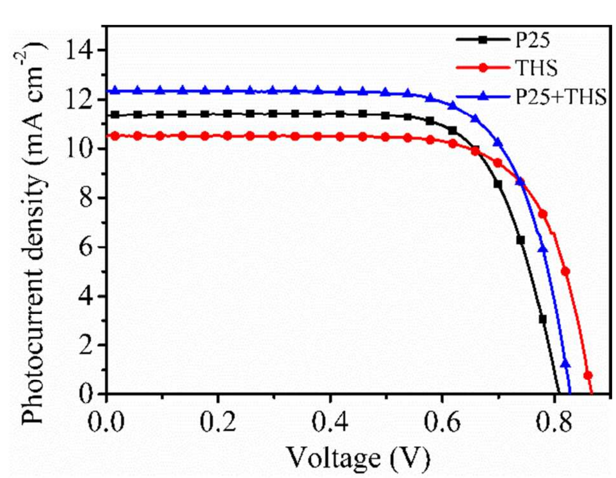

Fig. 6 The photocurrent-voltage curves of the DSSCs based on different working electrodes (Film P25, Film THS and Film P25+THS) measured under the illumination of one sun (AM 1.5 G, 100 mW cm^{-2}).

Table 1 Detailed photovoltaic parameters of cells based on different working electrodes measured under AM 1.5 G one sun illumination. J_{sc}: short-circuit photocurrent density; V_{oc}: open-circuit photovoltage; *FF*: fill factor; η: photovoltaic conversion efficiency

Cell	Dye absorption ($\times10^{-8}$ mol cm^{-2})	J_{sc} (mA cm^{-2})	V_{oc} (V)	*FF* (%)	η (%)
P25	15.9	11.34	0.809	72.48	6.65
THS	11.4	10.51	0.865	72.41	6.59
P25+THS	13.3	12.35	0.834	71.48	7.36

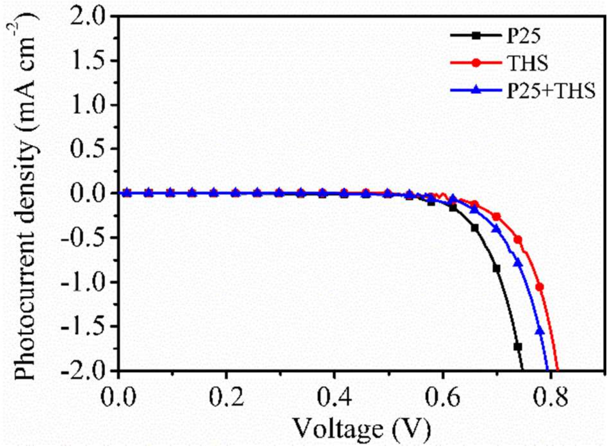

Fig. 7 Dark currents as a function of applied bias for three DSSCs.

The amount of adsorbed N719 dye was investigated and summarized in Table1. The dye loading amount was also a factor attributing to charge harvesting efficiency (η_{lh}) and relating to J_{sc}. The dye loading results show that the amount of dye adsorbed on hierarchically porous N-F codoped TiO_2 hollow sphere photoelectrode (Film THS: 11.4×10^{-8} mol cm^{-2}) is lower than that of the commercial P25 photoelectrode (Film P25: 15.9×10^{-8} mol cm^{-2}). This is attributed to the commercial P25 nanoparticles possess a larger specific surface area (54.214 m^2 g^{-1}) compared with hierarchically porous N-F codoped TiO_2 hollow spheres (29.845 m^2 g^{-1}) when the thicknesses are same. It should be noted that the J_{sc} of Cell THS comes close to that of Cell P25, in spite of the fact that Film THS adsorbs less dye compared to that of Film P25, implying that the hierarchically porous N-F codoped TiO_2 hollow spheres possess stronger light scattering ability than that of P25 nanoparticles. Moreover, the multiple-reflection effect occurring inside the interior cavities could trap the incident light in the photoanode for a longer duration, which brought forth more opportunities for light absorption. Compared with Cell P25, Cell P25+THS had a higher J_{sc}, because of the greater scattering effect of hierarchically porous N-F codoped TiO_2 hollow spheres, leading to enhance η of Cell P25+THS.

In order to investigate the light scattering property of the three films, the UV-Vis reflectance spectra are further characterized and shown in Fig. 8. The commercial P25 film fabricated from nanometer-sized crystallites exhibits a weak scattering effect and a large portion of visible light in the long-wavelength region transmitted through the film directly. Whereas the reflectance capacity of film THS is 50-65% in the visible range, which is much higher than that of P25 film. This can be explained by light scattering of the hierarchically porous N-F codoped TiO_2 hollow spheres, because the particle size of the hierarchical N-F codoped TiO_2 hollow spheres is analogous to the wavelength of visible light, which can lead to a strong scattering effect according to Mie theory.[32] The hierarchical N-F codoped TiO_2 hollow spheres have more suitable structures for light scattering than the P25 nanocrystallites. The bilayer film consists of both P25 nanocrystallites and hierarchically porous N-F codoped TiO_2 hollow spheres, and therefore the intensity of diffuse reflectance of it falls between the hierarchically porous N-F codoped TiO_2 hollow spheres and P25 films. The light scattering can extend the distance of light travelled within the films. Such increased travelling distance within the photoelectrodes leads to increase photoabsorption, which would enhance the probability of photons being captured by the dye molecules. Therefore, it is deduced that the enhanced η of Cell P25+THS is closely related with strong light scattering ability.

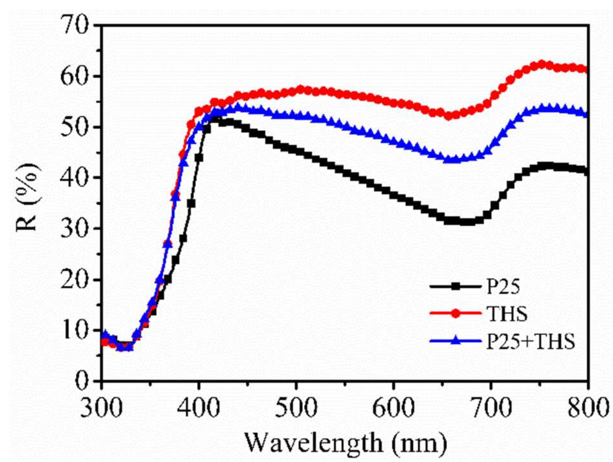

Fig. 8 Diffuse reflectance spectra of the three photoanode films.

The photocurrent responses of the DSSCs based on different photoanodes were compared via IPCE measurements. As shown in Fig. 9, Cell P25+THS demonstrates apparently higher IPCE peaks at 530 nm over Cell P25 and Cell THS. It is worth noting that the IPCE data of Cell-THS and Cell P25+THS show an obvious red-shift to a longer wavelength (600-750 nm) compared to Cell P25 due to the better light scattering ability for N-F codoped TiO_2 hollow spheres. Compared to Cell P25, Cell-THS exhibits a lower IPCE which should be a result of the lower amount of dye anchored onto the N-F codoped TiO_2 hollow sphere photoanode. Considering the lower dye loading capacities of Film P25-THS photoanode, the higher IPCE values are mainly attributed to the scattering effect of N-F codoped TiO_2 hollow spheres, which substantially improves the light harvesting of N719 dye.

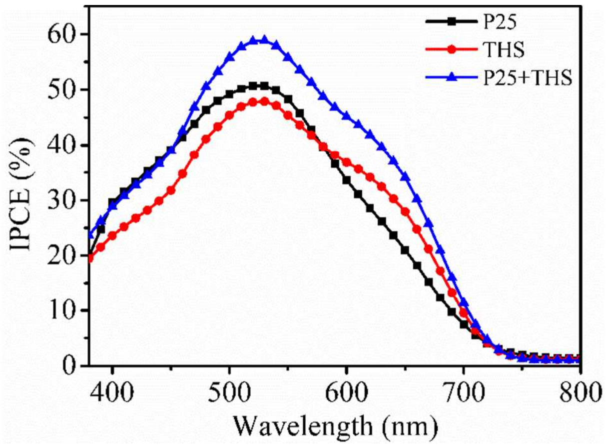

Fig. 9 IPCE spectra of cells based on P25, THS and P25+THS.

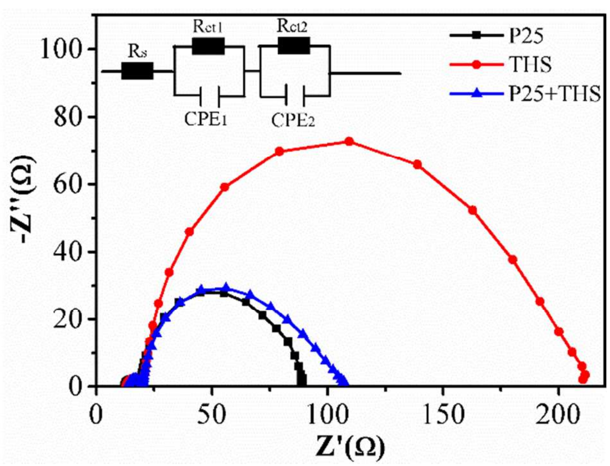

Fig. 10 Nyquist plots of DSSCs based on different photoanodes (P25, THS and P25+THS) measured in the dark at -0.83 V bias. And the inset illustrates the equivalent circuit simulated to fit the impedance spectrum.

Table 2 Series resistance (R_s), charge transfer resistance (R_{ct1}), and electron transfer and recombination (R_{ct2}) of the DSSCs fabricated using different photoanodes

Cell	R_s (Ω)	R_{ct1} (Ω)	R_{ct2} (Ω)	τ (ms)
P25	11.87	7.52	69.33	78
THS	13.66	6.55	178.9	171
P25+THS	14.64	5.77	79.18	101

For further insight into charge transport and recombination kinetics of three cells, electrochemical impedance spectroscopy (EIS) has been carried out. To reveal the difference in the interfacial characteristics of these photoelectrodes, we measured EIS spectra of the DSSCs at an applied bias of -0.83 V and a frequency range from 10 mHz to 1 MHz, with AC amplitude of 10 mV in the dark. Fig. 10 shows the typical EIS Nyquist plots of DSSCs with P25, THS, and P25+THS, respectively. The results reveal that all spectra are composed of two semicircles with a small one in the high-frequency region and a large one in the low-frequency region. The small semicircle represents the charge transfer resistance (R_{ct1}) corresponding with the charge transfer process occurring at the interface between the counter electrode and the electrolyte containing redox couple I^-/I_3^-.[4, 22] The large semicircle originates from the charge transfer and recombination resistance (R_{ct2}) related to the electron transport process within theTiO_2 films and the charge transfer process at the TiO_2/dye/electrolyte interfaces.[4, 22] An equivalent circuit as given in the inset of Fig. 10 was adopted to fit the EIS data. Shown in the equivalent circuit, R_s represents the series ohmic resistance existing in the external circuit, and *CPE* is constant phase element resulting from the capacitor components in the solar cell. The R_s, R_{ct1}, and R_{ct2} values fitted by Z-view software using the equivalent circuit are listed in Table 2. The three cells show similar R_s and R_{ct1}, leading to similar *FF* because the same electrolyte and counter electrode were used. However, the R_{ct2} value of Cell P25, Cell THS and Cell P25+THS is 69.33, 178.9 and 79.18 Ω, respectively. This result suggests that Cell THS retards the charge recombination, that is, a more effective suppression of the back reaction of the injected electron with the I_3^- in the electrolyte by decreasing the surface charge trap-site density of the Cell THS. The product of the charge-transfer resistance and the chemical capacitance corresponds to the electron lifetime, $\tau = CPE\text{-}T \times R$, we are able to extract information on electron lifetime. As displayed in Table 2, the τ values of Cell P25, Cell THS and Cell P25+THS is 78, 171 and 101 ms, respectively. Cell THS has a longer τ than Cell P25+THS and Cell P25. The prolonged τ for hierarchically porous TiO_2 hollow spheres based DSSC (Cell THS) could allow more effective electron transport and leads to a higher V_{oc}. This result agrees well with the *J-V* data.

4. Conclusion

In summary, we have successfully prepared the porous N-F codoped TiO_2 hollow spheres by a facile hydrothermal method involving use of CO_2 bubbles generated in situ from the decomposition of urea. The porous N-F codoped TiO_2 hollow spheres have a diameter of about 0.8-1.8 μm and a specific surface area of 29.845 m^2 g^{-1}. The optical investigation evidences that the porous N-F codoped TiO_2 hollow sphere film has a prominent light scattering effect at a wavelength range of 600-800 nm. The hollow structure improves electrolyte diffusion ability and enhances the light scattering effect. Furthermore, we use these porous N-F codoped TiO_2 hollow spheres as the scattering layer to balance the dye adsorption and scattering effect in DSSCs and a 7.36% solar energy conversion efficiency is demonstrated. The efficiency of DSSCs made from porous N-F codoped TiO_2 hollow spheres as the scattering layer is higher than that of DSSC made from the monolayer P25 due to the effective suppression of the back reaction of the injected electron with the I_3^- in the electrolyte by decreasing the surface charge trap-site density of the photoanode and excellent light scatter ability.

Acknowledgements

This work is supported by the National Natural Science Foundation of China (21365010), the Nature Science Foundation of Hainan Province (213015), the Project of Hainan Applied Technology Research and Development (ZDXM2014098) and the Undergraduate Training Programs for Innovation and Entrepreneurship (cxcyxj201414).

Notes and references

School of Chemistry and Chemical Engineering, Hainan Normal University, Haikou 571158, P. R. China.

*E-mail: sun@hainnu.edu.cn; Fax: +86 898 31381637; Tel: +86 898 31381637

1 B. O'Regan and M. Grätzel, *Nature*, 1991, **353**, 737-740.
2 S. Mathew, A. Yella, P. Gao, R. Humphry-Baker, B. F. E. Curchod, N. Ashari-Astani, I. Tavernelli, U. Rothlisberger, M. K. Nazeeruddin and M. Grätzel, *Nature Chem.*, 2014, **6**, 242-247.
3 J. F. Yan and F. Zhou, *J. Mater. Chem.*, 2011, **21**, 9406-9418.
4 B. X. Lei, Q. P. Luo, X. Y. Yu, W. Q. Wu, C. Y. Su and D. B. Kuang, Phys. Chem. Chem. Phys., 2012, 14, 13175-13179.
5 Y. P. Liu, S. R. Wang, Z. Q. Shan, X. G. Li, J. H. Tian, Y. M. Mei, H. M. Ma and K. L. Zhu. *Electrochim. Acta*, 2012, **60**, 422-427.
6 W. Shao, F. Gu, L. L. Gai and C. Z. Li, *Chem. Commun*., 2011, **47**, 5046-5048.
7 J. F. Qian, P. Liu, Y. Xiao, Y. Jiang, Y. L. Cao, X. P. Ai and H. X. Yang, *Adv. Mater*., 2009, **21**, 3663-3367.
8 Z. H. Dong, X. Y. Lai, J. E. Halpert, N. L. Yang, L. X. Yi, J. Zhai, D. Wang, Z. Y. Tang and L. Jiang, *Adv. Mater*., 2012, **24**, 1046-1049.
9 H. J. Koo, Y. J. Kim, Y. H. Lee, W. I. Lee, K. Kim and N. G. Park, *Adv. Mater*., 2008, **20**, 195-199.
10 D. P. Wu, F. Zhu, J. M. Li, H. Dong, Q. Li, K. Jiang and D. S. Xu, *J. Mater. Chem.,* 2012, **22**, 11665-11671.
11 L. Song, H. B. Yang, X. Wang, S. Y. Khoo, C. C. Wong, X. W. Liu and C. M. Li, *ACS Appl. Mater. Interfaces,* 2012, **4**, 3712-3717.
12 S. Dadgostar, F. Tajabadi and N. Taghavinia, *ACS Appl. Mater. Interfaces,* 2012, **4**, 2964-2968.
13 X. Wu, G. Q. Lu and L. Z. Wang, *Energy Environ. Sci,.* 2011, **4**, 3565-3572.
14 G. J. Ke, H. Y. Chen, C. Y. Su and D. B. Kuang, *J. Mater. Chem. A,* 2013, **1**, 13274-13282.
15 J. C. Huo, Y. J. Hu, H. Jiang, W. J. Huang, Y. F. Li, W. Shao and C. Z. Li, *Ind. Eng. Chem. Res.,* 2013, **52**, 11029-11035.
16 Z. Y. Zhong, Y. D. Yin, B. Gates and Y. N. Xia, *Adv. Mater,.* 2000, **12**, 206-209.
17 R. A. Caruso, A. Susha and F. Caruso, *Chem. Mater.,* 2001, **13**, 400-409.
18 X. M. Sun, J. F. Liu and Y. D. Li, *Chem. Eur. J.,* 2006, **12**, 2039-2047.
19 Z. Kai, X. H. Zhang, H. T. Chen, C. Xin, L. L. Zheng, J. H. Zhang and Y. Bai, *Langmuir,* 2004, **20**, 11312-11314.
20 T. Z. Ren, Z. Y. Yuan and B. L. Su, *Chem. Phys. Lett.,* 2003, **374**, 170-175.
21 A. M. Collins, C. Spickermann and S. Mann, *J. Mater. Chem.,* 2003, **13**, 1112-1114.
22 B. X. Lei, W. J. Fang, Y. F. Hou, J. Y. Liao, D. B. Kuang and C.Y. Su, *J. Photochem. Photobiol. A: Chem.,* 2010, **216**, 8-14.
23 N. G. Park, M. G. Kang, K. S. Ryu, K. M. Kim and S. H. Chang, *J. Photochem. Photobiol. A: Chem.,* 2004, **161**, 105-110.
24 W. Q. Jiang, Z. Cao, R. Gu, X. Z. Ye, C. F. Jiang and X. L Gong, *Smart. Mater. Struct.,* 2009, **18**, 125013-125016.
25 J. X. Sun, G. Chen, J. Z. Wu, H. J. Dong and G. H. Xiong, *Appl. Catal. B: Environ.,* 2013, **132**, 304-314.
26 C. Zhou, Y. F. Zhao, T. Bian, L. Shang, H. J. Yu, L. Z. Wu, C. H. Tung and T. R. Zhang, *Chem. Commun.,* 2013, **49**, 9872-9874.
27. X. W. Lou, L. A. Archer and Z. C. Yang, *Adv. Mater.,* 2008, **20**, 3987-4019.
28 J. G. Yu, G. H. Wang, B. Cheng and M. H. Zhou, *Appl. Catal. B: Environ.,* 2007, **69**, 171-180.
29 J. G. Yu, L. J. Zhang, B. Cheng and Y. R. Su, *J. Phys. Chem. C,* 2007, **111**, 10582-10589.
30 J. G. Yu, J. J. Fan and B. Cheng, *J. Power Sources,* 2011, **196**, 7891-7898.
31 J. H. Park, S. Y. Jung, R. Kim, N. G. Park, J. Kim and S. S. Lee, *J. Power Sources,* 2009, **194**, 574-578.
32 F. Z. Huang, D. H. Chen, X. L. Zhang, R. A. Caruso and Y. B. Cheng, *Adv. Funct. Mater.,* **2010**, 20, 1301-1305.

TOC

Hierarchically porous N-F codoped TiO_2 hollow spheres were prepared via an in situ bubbling method for solar energy conversion application.